D_2 Hyperfine Structure of Rubidium Isotopes ^{87}Rb and ^{85}Rb

Bhaskar Mookerji and Charles Herder*
MIT Department of Physics
(Dated: April 6, 2008)

We experimentally characterize the hyperfine structure of $D2$ (near 780nm) transition in ^{87}Rb ($I = 3/2$) and ^{85}Rb ($I = 5/2$). Using an AlGaAs diode laser, we perform laser-saturation spectroscopy to eliminate the effects of doppler broadening our spectra. The hyperfine splittings are measured, and the magnetic dipole (A) and electric quadrapole (B) hyperfine coupling constants of the $5^2S_{1/2}$ and $5^2P_{3/2}$ states are determined within experimental error of accepted values.

Characterizing atomic structure beyond the Bohr energies and fine structure perturbations is a seemingly prohibitive task when faced with the Doppler broadening of spectral lines. Laser-saturation spectroscopy is used to achieve spectral resolution well-below the Doppler broadening found in typical optical spectra. Monochromatic laser beams from a common diode source traveling in opposite directions pass through a sample gas absorption tube. The beams (*pump* and *probe*) differ significantly in intensity, and when the laser is tuned near the frequency of the atomic hyperfine transitions, the probe beam transmission exhibits a Lorentzian decay profile characteristic of the natural line width of the transition.

Our purpose is to use this technique to describe the hyperfine structure of the optical valence electron in a rubidium atom with ground state electronic structure [Kr]5s^1. In the following we will first describe the perturbations that contribute to rubidium's hyperfine structure. We will also implement saturation absorption-spectroscopy to eliminate the doppler broadening masking hyperfine splitting, and discuss nuclear coupling and isotope effects.

1. HYPERFINE STRUCTURE

Determining the hyperfine coupling constants requires that we understand the magnitude of the hyperfine splittings. The principal energy levels of the Bohr Hamiltonian treat the nucleus as a point-mass of a spherically-symmetric Coulomb potential: adding perturbations to this Hamiltonian removes the degeneracy of the principal energy levels. Fine structure corrections resolve the ground state ($5^2S_{1/2}$) and split first excited states ($5^2P_{1/2}$ and $5^2P_{3/2}$) labeled by $|njm_j\rangle$, where $\mathbf{J} = \mathbf{L}+\mathbf{S}$ is the total angular momentum of the optical electron. Transitions between the ground and first excited states occur at 794nm and 780nm, respectively

Hyperfine structure is due to the magnetic dipole and electric quadrapole interactions of the optical electron with the the nuclear spins $\mathbf{I}$ of ^{87}Rb ($I = 3/2$) and ^{85}Rb ($I = 5/2$)[1]. Like the fine structure interaction, the magnetic moment $\mu_\mathbf{I}$ of the nucleus couples to the magnetic field $\mathbf{B}_{el}$ produced at the nucleus by the electron,

$$H^{hf}_{magn} = -\mu_I \cdot \mathbf{B}_{el} \rightarrow A\mathbf{I}\cdot\mathbf{J}, \tag{1}$$

where electron's magnetic field is proportional the angular momentum $\mathbf{J}$, and A parametrizes the strength of the magnetic dipole interactions. The electron and nuclear angular momenta are coupled together to a total angular momentum $\mathbf{F}$ for the atom. In terms of a complete set of commuting observables labeled by $|IJFm_F\rangle$, the magnetic dipole spectrum is given by

$$\Delta E^{hf}_{magn} = \langle H^{hf}_{magn}\rangle = \frac{1}{2}AC, \tag{2}$$

where $C = F(F+1) - J(J+1)F - I(I+1)$.

Expanding the electrostatic interaction of the optical electron and the protons of the rubidium nucleus in terms of spherical harmonics yields the remaining contribution,

$$H^{hf}_{quad} = B\frac{3(\mathbf{I}\cdot\mathbf{J})^2 + \frac{3}{2}\mathbf{I}\cdot\mathbf{J} - I(I+1)J(J+1)}{2I(2I-1)J(2J-1)}, \tag{3}$$

where B specifies the gradient of the electric quadrapole potential. The major electrical pole of the rubidium is the spherically symmetric electric monopole in the Bohr Hamiltonian, so $B = 0$ for spherically symmetric angular momentum states. The total hyperfine corrections the $n^{2s+1}L_j$ state are then,

$$\Delta E_F = \frac{1}{2}AC + B\frac{\frac{3}{4}C(C+1) - I(I+1)J(J+1)}{2I(2I-1)J(2J-1)}. \tag{4}$$

For hyperfine states labeled between $F = |I+J|$ to $F = |I-J|$, allowed transitions give rise to observable spectra based on the angular momentum selection rules $\Delta F = 0, \pm 1$.

1.1. Doppler-Free Spectroscopy

An atom of mass A moving relative to a laser source of frequency ν_0 sees blue or red shifted radiation. Moreover, at a finite temperature T, their velocities will be Maxwell-Boltzmann distributed and the resulting absorption profile of our spectra will have a full-width at half-maximum

*Electronic address: mookerji@mit.edu; URL: http://web.mit.edu/8.13/

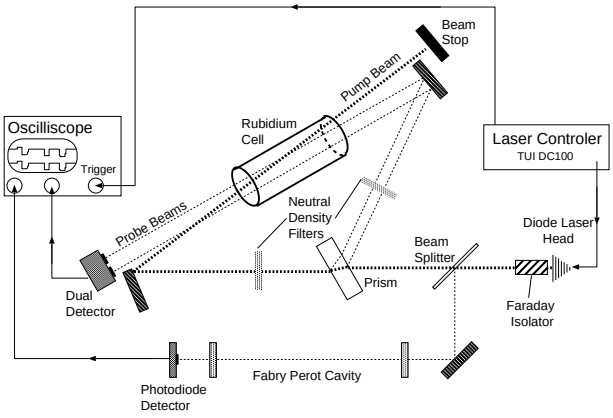

FIG. 1: Table schematic for performing saturation-absorption spectroscopy. A Faraday isolator at the output of the laser head acts as an optical diode, preventing back reflections into the laser head.

(FWHM) of

$$\Delta\nu_{1/2} = 2\frac{\nu_0}{c}\sqrt{\frac{2k_BT\ln 2}{A}}. \tag{5}$$

For a sample of rubidium atoms at 297K being driven at 780nm, this width is approximately 502MHz, far larger than the natural line width of hyperfine transitions at 6.059(6)MHz.

Saturation absorption spectroscopy can be thought of by examining a two-state system with ground and excited states $|g\rangle$ and $|e\rangle$ interacting with the pump and probe beams mentioned earlier. The probe beam alone demonstrates a typical Gaussian absorption profile, however the addition of a more intense pump beam moving opposite the probe will also be seen (at the same frequency!) by atoms moving at zero velocity. Atoms moving relative to the beams will see radiation Doppler-shifted from resonance. The high intensity of the pump beam leads to a high absorption rate as the atoms undergo a transition from $|g\rangle$ to $|e\rangle$, and the resulting absorption of the lower intensity probe beam is significantly reduced, resulting in a spike (or *Lamb dip*) in the Doppler spectrum at the resonant frequency of the hyperfine transition.

2. EXPERIMENTAL SETUP AND PROCEDURE

A table schematic of the optical arrangement for this experiment is in Figure 1. A DL100 Tui Optics external cavity diode laser is our light source. The laser head contains a 780nm AlGaAs laser diode, a collimating lens mounted on a temperature-controlled stage, and a diffraction grating that allows us to finely tune the output frequency of the laser diode. The output frequency and power of the laser diode is single mode and is controlled by diode temperature (18.0°C) and current bias (about 55 mA). This frequency can be swept through the atomic transition lines by varying the amplitude and frequency of a periodic voltage ramp across a piezoelectric transducer, thereby changing the length of the laser diode cavity.

Following the Faraday isolator, a glass slide splits the beam into an optional Fabry-Perot interferometer (see Section 2.1) and our primary measurement setup. The main beam is passed through a 90:10 beamsplitting prism into a pump beam and two probe beams, each of which passes though a variable neutral density filter to reduce the laser power broadening of the Rb spectral lines[1]. Two mirrors reflect the pump and probe beams toward each other, passing through the rubidium cell, where only one probe beam intersects with the pump beam. The two probe beams are fed into a photodiode-based balanced detector, which measures the intensity difference between the Doppler broadened and Lamb dip spectra and leaves the inverted Lamb dip as a Doppler-free spectral peak captured by an 60MHz Agilent 54621A oscilloscope.

2.1. Fabry-Perot Calibration

In order to measure the hyperfine splittings, a reference frequency is required to scale the time abscissa on the oscilloscope in terms of frequency. The Fabry-Perot interferometer consists of two partially-reflective mirrors forming an optical cavity of length L (see Figure 1) through which the laser beam can oscillate back and forth. The resulting interference pattern is measured with a photodiode. The frequency spacing between two adjacent transmission modes is called the *free spectral range* and is given by,

$$\Delta\nu = \frac{c}{2n_{\text{Air}}L}, \tag{6}$$

where c is the speed of light and n_{Air} is the index of refraction of air. The measured mirror separation was $L = 70.0 \pm 0.5$cm, and the free spectral range was $\Delta\nu = 214 \pm 2$MHz. The relative spacing of the spectral transitions can be determined by comparing the interferometer and measured spectra, as the period of the intensity interference is related to the frequency of the laser.

3. RESULTS AND ERROR ANALYSIS

The measured Doppler spectrum and Lamb dips from the balanced detector are given in Figure 2, to which we attribute random error and systematic line broadening contributions. In the analysis of the hyperfine splittings, there are several sources of error that we account

[1] Ideally, because the ^{87}Rb and ^{85}Rb isotopes differ in abundance, one would want to use a combination of different neutral density filters to acquire spectra for different transition groups.

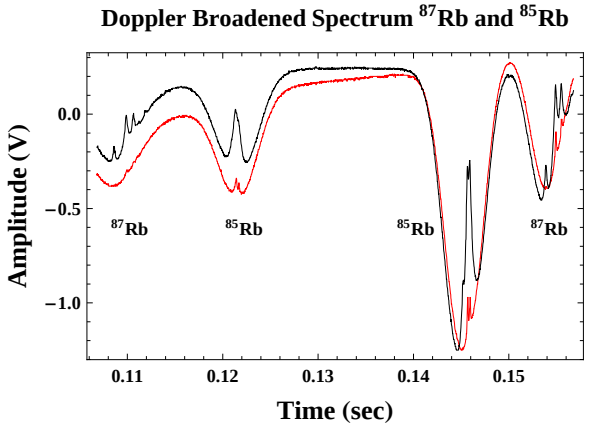

FIG. 2: Doppler broadened spectra of ^{87}Rb and ^{85}Rb fine structure. One probe beam input into the balanced detector exhibits Lamb dips at the hyperfine transition frequencies.

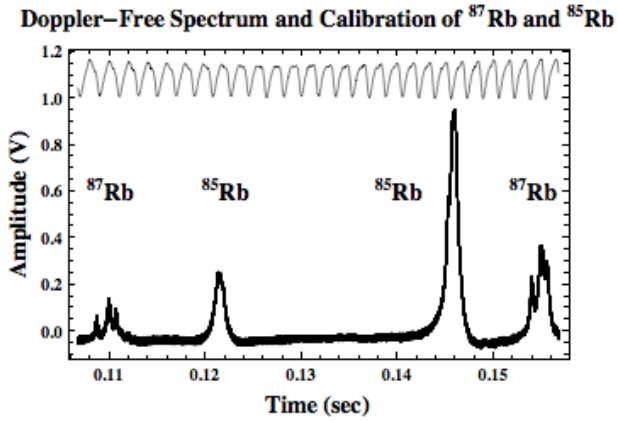

FIG. 3: Full Doppler-free spectra. Note the mode mixing of the Fabry-Perot trace.

for in each of our points. Error is propagated from our measurement of the interferometer cavity length, a background noise of 5-10mV from the limitations of the oscilloscope's resolution and the mechanical sensitivity of our optical setup, and the nonlinear sweep of the Fabry-Perot. The spectrum of our Fabry-Perot trace also reveals three, equally-spaced resonances of decreasing amplitude, indicating that our laser diode was operating at multiple modes. Using the center frequencies of the resonances, we fit a sum of sine waves to Fabry-Perot trace and added a proportional error to the hyperfine center frequency in a given period of the trace.

The spontaneous decay lifetime τ of the excited state and Heisenberg uncertainty suggest that hyperfine spectra have a Lorentzian linewidth of $1/2\pi\tau$, or 6.059(6)MHz for rubidium. However, there are several random decay processes adding Lorentzian line broadening to the natural line width of our measurements. The major sources of broadening are the MHz power broadening from laser intensity, which is dependent on the rate at which the laser light stimulates the observed transitions; and the limited laser linewidth $\delta\nu \approx 30$MHz curtailing our resolving power. Close to a sample gas pressure of 1 mTorr, inter-atom collisions result in phase shifts and subsequent state decay, contributing a broadening on the order of 10^5Hz. When the cross-sectional area of the cell is on the order of centimeters, particle-wall collisions induce line broadening on the order of 10^4Hz[2].

3.1. Hyperfine Structure of Rubidium

Using the saturation spectroscopy method, we measured the $5^2S_{1/2}$ and $5^2P_{3/2}$ hyperfine spectra for ^{87}Rb and ^{85}Rb and fit the resonances with Lorentzians on linearly decaying backgrounds (with acceptable χ^2_ν values) using the Lev-Marquardt fitting algorithm in Mathematica 6. A figure for the entire background-subtracted

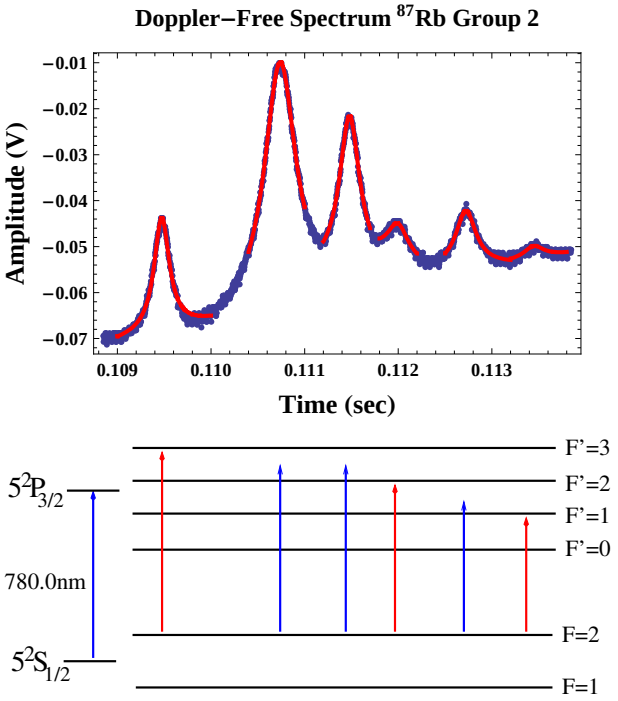

FIG. 4: ^{87}Rb hyperfine spectra from $5^2S_{1/2}\,(F=2)$. The spectra is fit piecewise with Lorentzians with an approximately linearly decaying background signal. The corresponding hyperfine and crossover transitions are labeled below.

spectrum is in Figure 3. Examples spectra for ^{87}Rb and ^{85}Rb and are included in Figures 4 and 5. The full spectrum includes four sets of six resonances with a measured linewidth of 14 ± 2MHz, significantly smaller than the Doppler-broadened linewidth. Higher frequency transitions from the lower of the hyperfine substates start from the left, where we set an arbitrary zero-frequency reference point. Several characteristics of these spectra are important. The increased intensity of the ^{85}Rb groups

TABLE I: Classification of hyperfine structure for ^{87}Rb and ^{85}Rb isotopes.

	Transition	$\Delta\nu_{\text{Pub.}}$(MHz)[3]	$\Delta\nu_{\text{Meas.}}$(MHz)
^{87}Rb	$5^2P_{3/2}\,(F=3,2)$	266.7	268.0 ± 2.0
	$5^2P_{3/2}\,(F=2,1)$	156.9	155.0 ± 5.7
	$5^2P_{3/2}\,(F=1,0)$	72.2	65.3 ± 7.0
	$A\,(5^2P_{3/2})$	84.5	84.3 ± 1.8
	$B\,(5^2P_{3/2})$	12.5	16.2 ± 5.1
	$5^2S_{1/2}\,(F'=2,1)$	6834.7	6712.9 ± 167.5
	$A\,(5^2S_{1/2})$	3417.3	3360 ± 84
^{85}Rb	$5^2P_{3/2}\,(F=4,3)$	121	110.8 ± 8.8
	$5^2P_{3/2}\,(F=3,2)$	63	67.7 ± 4.1
	$5^2P_{3/2}\,(F=2,1)$	29	32.7 ± 3.0
	$A\,(5^2P_{3/2})$	25.1	24.4 ± 2.0
	$B\,(5^2P_{3/2})$	25.9	17.5 ± 7.5
	$5^2S_{1/2}\,(F'=3,2)$	3036	2905.96 ± 115.3
	$A\,(5^2S_{1/2})$	1011.9	970 ± 38

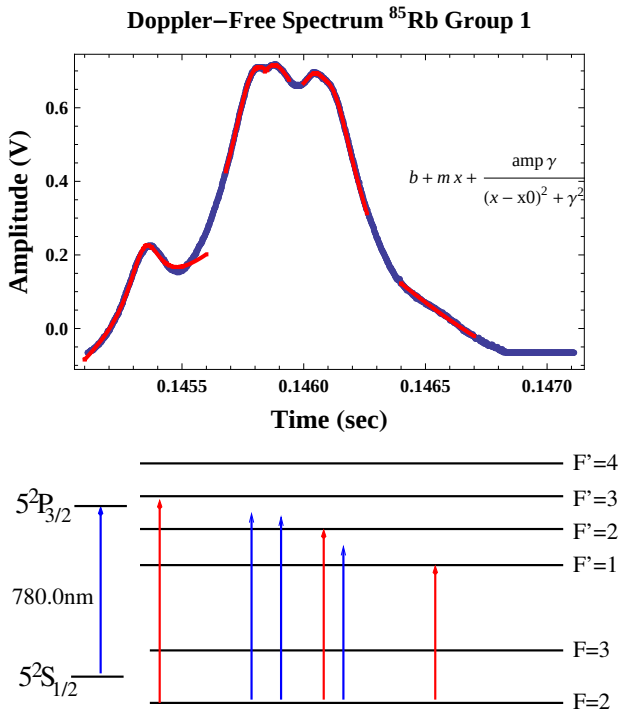

FIG. 5: ^{85}Rb hyperfine spectra from $5^2S_{1/2}\,(F=2)$. The spectra is fit piecewise with Lorentzians with an approximately linearly decaying background signal. The corresponding hyperfine and crossover transitions are labeled below.

relative to the ^{87}Rb groups can be attributed to the greater isotope abundance of ^{85}Rb, whereas the increased hyperfine splitting in the ^{87}Rb groups can be attributed to the greater nuclear magnetic moment of the ^{87}Rb nucleus. Hyperfine splittings between the F states are determined by determining the relative frequency difference between pairs of transitions with common initial or final states, for which the resulting values (Table I) are typically within a standard deviation of published values. The measured hyperfine splitting for the $5^2S_{1/2}$ is taken from transitions between different fine structure groups, resulting in a larger propogated error over many periods of the Fabry-Perot trace. Hyperfine coupling constants are interpolated from Equation 4.

The crossover resonances in our spectra are peculiar to the method of saturation-absorption spectroscopy. Such a transition occurs between any two transitions ν_1 and ν_2 that share a common ground state and differ in frequency by less than the Doppler linewidth. For any two transitions, a laser frequency at ν_c is seen by atoms moving with velocity v into the probe beam as being redshifted to a transition frequency ν_2, and similarly to ν_1 for the pump beam. The doppler shifts for the pump and probe beams

$$\nu_1 = \nu_c - \frac{v}{c}\nu_c \qquad \text{and} \qquad \nu_2 = \nu_c + \frac{v}{c}\nu_c, \tag{7}$$

can be solved the crossover frequency ν_c

$$\nu_c = \frac{1}{2}\left(\nu_1 + \nu_2\right) \tag{8}$$

which occurs halfway between any two hyperfine transitions. Using this, hyperfine transitions that are not resolved in our spectra of ^{85}Rb are interpolated from their corresponding crossover transitions. These crossover resonances also interpolated transitions for which a given peak was upside down, an effect that can accounted for by hyperfine optical pumping[2].

3.2. Conclusion

In summary, we have characterized and measured the hyperfine structure and coupling constants of the ^{87}Rb and ^{85}Rb isotopes by eliminating the Doppler-broadening effects found in linear laser spectroscopy. Our measured values are typically within one standard deviation of published values. In the future, the effects of polarization spectroscopy may further increase the resolution of these measurements, and the Junior Lab staff might consider investing in infrared polarizing filters for such explorations. [4]

[1] G. Woodgate, *Elementary Atomic Structure* (Oxford University Press, 1980).
[2] V. Letokhov and V. Chebotayev, *Nonlinear Laser Spectroscopy* (Springer-Verlag, New York, 1977).
[3] M. I. E. Arimondo and P. Violino, Rev. Mod. Phys. **49**, 39 (1977).
[4] C. Wieman and T. Hansch, Phys. Rev. Lett. **36**, 1170 (1976).